

Faculty Publications

9-2016

Study of Two-Body $e+e\rightarrow B(*)sB^-(*)s$ Production in the Energy Range from 10.77 to 11.02 GeV

A. Abdesselam et al.

Belle Collaboration

David Joffe

Kennesaw State University, djoffe@kennesaw.edu

Ratnappuli L. Kulasiri

Kennesaw State University, rkulasir@kennesaw.edu

Follow this and additional works at: <https://digitalcommons.kennesaw.edu/facpubs>



Part of the [Physics Commons](#)

Recommended Citation

et al., A. Abdesselam; Joffe, David; and Kulasiri, Ratnappuli L., "Study of Two-Body $e+e\rightarrow B(*)sB^-(*)s$ Production in the Energy Range from 10.77 to 11.02 GeV" (2016). *Faculty Publications*. 4214.
<https://digitalcommons.kennesaw.edu/facpubs/4214>

Study of Two-Body $e^+e^- \rightarrow B_s^{(*)}\bar{B}_s^{(*)}$ Production in the Energy Range from 10.77 to 11.02 GeV

A. Abdesselam,⁹² I. Adachi,^{20,16} K. Adamczyk,⁶⁶ H. Aihara,¹⁰⁰ S. Al Said,^{92,42}
 K. Arinstein,^{5,70} Y. Arita,⁵⁹ D. M. Asner,⁷³ T. Aso,¹⁰⁵ H. Atmacan,⁵⁵ V. Aulchenko,^{5,70}
 T. Aushev,⁵⁸ R. Ayad,⁹² T. Aziz,⁹³ V. Babu,⁹³ I. Badhrees,^{92,41} S. Bahinipati,²⁶
 A. M. Bakich,⁹¹ A. Bala,⁷⁴ Y. Ban,⁷⁵ V. Bansal,⁷³ E. Barberio,⁵⁴ M. Barrett,¹⁹
 W. Bartel,¹⁰ A. Bay,⁴⁷ I. Bedny,^{5,70} P. Behera,²⁸ M. Belhorn,⁹ K. Belous,³² M. Berger,⁸⁹
 D. Besson,⁵⁷ V. Bhardwaj,²⁵ B. Bhuyan,²⁷ J. Biswal,³⁶ T. Bloomfield,⁵⁴ S. Blyth,⁶⁴
 A. Bobrov,^{5,70} A. Bondar,^{5,70} G. Bonvicini,¹⁰⁸ C. Bookwalter,⁷³ C. Boulaouache,⁹²
 A. Bozek,⁶⁶ M. Bračko,^{52,36} F. Breibeck,³¹ J. Brodzicka,⁶⁶ T. E. Browder,¹⁹ E. Waheed,⁵⁴
 D. Červenkov,⁶ M.-C. Chang,¹² P. Chang,⁶⁵ Y. Chao,⁶⁵ V. Chekelian,⁵³ A. Chen,⁶³
 K.-F. Chen,⁶⁵ P. Chen,⁶⁵ B. G. Cheon,¹⁸ K. Chilikin,^{48,57} R. Chistov,^{48,57} K. Cho,⁴³
 V. Chobanova,⁵³ S.-K. Choi,¹⁷ Y. Choi,⁹⁰ D. Cinabro,¹⁰⁸ J. Crnkovic,²⁴ J. Dalseno,^{53,94}
 M. Danilov,^{57,48} N. Dash,²⁶ S. Di Carlo,¹⁰⁸ J. Dingfelder,⁴ Z. Doležal,⁶ D. Dossett,⁵⁴
 Z. Drásal,⁶ A. Drutskoy,^{48,57} S. Dubey,¹⁹ D. Dutta,⁹³ K. Dutta,²⁷ S. Eidelman,^{5,70}
 D. Epifanov,¹⁰⁰ S. Esen,⁹ H. Farhat,¹⁰⁸ J. E. Fast,⁷³ M. Feindt,³⁸ T. Ferber,¹⁰
 A. Frey,¹⁵ O. Frost,¹⁰ B. G. Fulsom,⁷³ V. Gaur,⁹³ N. Gabyshev,^{5,70} S. Ganguly,¹⁰⁸
 A. Garmash,^{5,70} D. Getzkow,¹³ R. Gillard,¹⁰⁸ F. Giordano,²⁴ R. Glattauer,³¹ Y. M. Goh,¹⁸
 P. Goldenzweig,³⁸ B. Golob,^{49,36} D. Greenwald,⁹⁵ M. Grosse Perdekamp,^{24,81} J. Grygier,³⁸
 O. Grzymkowska,⁶⁶ H. Guo,⁸³ J. Haba,^{20,16} P. Hamer,¹⁵ Y. L. Han,³⁰ K. Hara,²⁰
 T. Hara,^{20,16} Y. Hasegawa,⁸⁵ J. Hasenbusch,⁴ K. Hayasaka,⁶⁸ H. Hayashii,⁶² X. H. He,⁷⁵
 M. Heck,³⁸ M. T. Hedges,¹⁹ D. Heffernan,⁷² M. Heider,³⁸ A. Heller,³⁸ T. Higuchi,³⁹
 S. Himori,⁹⁸ S. Hirose,⁵⁹ T. Horiguchi,⁹⁸ Y. Hoshi,⁹⁷ K. Hoshina,¹⁰³ W.-S. Hou,⁶⁵
 Y. B. Hsiung,⁶⁵ C.-L. Hsu,⁵⁴ M. Huschle,³⁸ H. J. Hyun,⁴⁶ Y. Igarashi,²⁰ T. Iijima,^{60,59}
 M. Imamura,⁵⁹ K. Inami,⁵⁹ G. Inguglia,¹⁰ A. Ishikawa,⁹⁸ K. Itagaki,⁹⁸ R. Itoh,^{20,16}
 M. Iwabuchi,¹¹⁰ M. Iwasaki,¹⁰⁰ Y. Iwasaki,²⁰ S. Iwata,¹⁰² W. W. Jacobs,²⁹ I. Jaegle,¹⁹
 H. B. Jeon,⁴⁶ Y. Jin,¹⁰⁰ D. Joffe,⁴⁰ M. Jones,¹⁹ K. K. Joo,⁸ T. Julius,⁵⁴ H. Kakuno,¹⁰²
 A. B. Kaliyar,²⁸ J. H. Kang,¹¹⁰ K. H. Kang,⁴⁶ P. Kapusta,⁶⁶ S. U. Kataoka,⁶¹ E. Kato,⁹⁸
 Y. Kato,⁵⁹ P. Katrenko,^{58,48} H. Kawai,⁷ T. Kawasaki,⁶⁸ T. Keck,³⁸ H. Kichimi,²⁰
 C. Kiesling,⁵³ B. H. Kim,⁸⁴ D. Y. Kim,⁸⁷ H. J. Kim,⁴⁶ H.-J. Kim,¹¹⁰ J. B. Kim,⁴⁴
 J. H. Kim,⁴³ K. T. Kim,⁴⁴ M. J. Kim,⁴⁶ S. H. Kim,¹⁸ S. K. Kim,⁸⁴ Y. J. Kim,⁴³
 K. Kinoshita,⁹ C. Kleinwort,¹⁰ J. Klucar,³⁶ B. R. Ko,⁴⁴ N. Kobayashi,¹⁰¹ S. Koblitz,⁵³

P. Kodyš,⁶ Y. Koga,⁵⁹ S. Korpar,^{52,36} D. Kotchetkov,¹⁹ R. T. Kouzes,⁷³ P. Križan,^{49,36}
P. Krokovny,^{5,70} B. Kronenbitter,³⁸ T. Kuhr,⁵⁰ L. Kulásíří,⁴⁰ R. Kumar,⁷⁷ T. Kumita,¹⁰²
E. Kurihara,⁷ Y. Kuroki,⁷² A. Kuzmin,^{5,70} P. Kvasnička,⁶ Y.-J. Kwon,¹¹⁰ Y.-T. Lai,⁶⁵
J. S. Lange,¹³ D. H. Lee,⁴⁴ I. S. Lee,¹⁸ S.-H. Lee,⁴⁴ M. Leitgab,^{24,81} R. Leitner,⁶ D. Levit,⁹⁵
P. Lewis,¹⁹ C. H. Li,⁵⁴ H. Li,²⁹ J. Li,⁸⁴ L. Li,⁸³ X. Li,⁸⁴ Y. Li,¹⁰⁷ L. Li Gioi,⁵³ J. Libby,²⁸
A. Limosani,⁵⁴ C. Liu,⁸³ Y. Liu,⁹ Z. Q. Liu,³⁰ D. Liventsev,^{107,20} A. Loos,⁸⁸ R. Louvt,⁴⁷
M. Lubej,³⁶ P. Lukin,^{5,70} T. Luo,⁷⁶ J. MacNaughton,²⁰ M. Masuda,⁹⁹ T. Matsuda,⁵⁶
D. Matvienko,^{5,70} A. Matyja,⁶⁶ S. McOnie,⁹¹ Y. Mikami,⁹⁸ K. Miyabayashi,⁶²
Y. Miyachi,¹⁰⁹ H. Miyake,^{20,16} H. Miyata,⁶⁸ Y. Miyazaki,⁵⁹ R. Mizuk,^{48,57,58}
G. B. Mohanty,⁹³ S. Mohanty,^{93,106} D. Mohapatra,⁷³ A. Moll,^{53,94} H. K. Moon,⁴⁴
T. Mori,⁵⁹ T. Morii,³⁹ H.-G. Moser,⁵³ T. Müller,³⁸ N. Muramatsu,⁷⁸ R. Mussa,³⁴
T. Nagamine,⁹⁸ Y. Nagasaka,²² Y. Nakahama,¹⁰⁰ I. Nakamura,^{20,16} K. R. Nakamura,²⁰
E. Nakano,⁷¹ H. Nakano,⁹⁸ T. Nakano,⁷⁹ M. Nakao,^{20,16} H. Nakayama,^{20,16} H. Nakazawa,⁶³
T. Nanut,³⁶ K. J. Nath,²⁷ Z. Natkaniec,⁶⁶ M. Nayak,^{108,20} E. Nedelkovska,⁵³ K. Negishi,⁹⁸
K. Neichi,⁹⁷ C. Ng,¹⁰⁰ C. Niebuhr,¹⁰ M. Niiyama,⁴⁵ N. K. Nisar,^{93,1} S. Nishida,^{20,16}
K. Nishimura,¹⁹ O. Nitoh,¹⁰³ T. Nozaki,²⁰ A. Ogawa,⁸¹ S. Ogawa,⁹⁶ T. Ohshima,⁵⁹
S. Okuno,³⁷ S. L. Olsen,⁸⁴ Y. Ono,⁹⁸ Y. Onuki,¹⁰⁰ W. Ostrowicz,⁶⁶ C. Oswald,⁴
H. Ozaki,^{20,16} P. Pakhlov,^{48,57} G. Pakhlova,^{48,58} B. Pal,⁹ H. Palka,⁶⁶ E. Panzenböck,^{15,62}
C.-S. Park,¹¹⁰ C. W. Park,⁹⁰ H. Park,⁴⁶ K. S. Park,⁹⁰ S. Paul,⁹⁵ L. S. Peak,⁹¹
T. K. Pedlar,⁵¹ T. Peng,⁸³ L. Pesáñez,⁴ R. Pestotnik,³⁶ M. Peters,¹⁹ M. Petrič,³⁶
L. E. Piilonen,¹⁰⁷ A. Poluektov,^{5,70} K. Prasanth,²⁸ M. Prim,³⁸ K. Prothmann,^{53,94}
C. Pulvermacher,³⁸ M. V. Purohit,⁸⁸ J. Rauch,⁹⁵ B. Reisert,⁵³ E. Ribežl,³⁶ M. Ritter,⁵⁰
J. Rorie,¹⁹ A. Rostomyan,¹⁰ M. Rozanska,⁶⁶ S. Rummel,⁵⁰ S. Ryu,⁸⁴ H. Sahoo,¹⁹ T. Saito,⁹⁸
K. Sakai,²⁰ Y. Sakai,^{20,16} S. Sandilya,⁹ D. Santel,⁹ L. Santelj,²⁰ T. Sanuki,⁹⁸ J. Sasaki,¹⁰⁰
N. Sasao,⁴⁵ Y. Sato,⁵⁹ V. Savinov,⁷⁶ T. Schlüter,⁵⁰ O. Schneider,⁴⁷ G. Schnell,^{2,23}
P. Schönmeier,⁹⁸ M. Schram,⁷³ C. Schwanda,³¹ A. J. Schwartz,⁹ B. Schwenker,¹⁵ R. Seidl,⁸¹
Y. Seino,⁶⁸ D. Semmler,¹³ K. Senyo,¹⁰⁹ O. Seon,⁵⁹ I. S. Seong,¹⁹ M. E. Sevier,⁵⁴
L. Shang,³⁰ M. Shapkin,³² V. Shebalin,^{5,70} C. P. Shen,³ T.-A. Shibata,¹⁰¹ H. Shibuya,⁹⁶
N. Shimizu,¹⁰⁰ S. Shinomiya,⁷² J.-G. Shiu,⁶⁵ B. Shwartz,^{5,70} A. Sibidanov,⁹¹ F. Simon,^{53,94}
J. B. Singh,⁷⁴ R. Sinha,³³ P. Smerkol,³⁶ Y.-S. Sohn,¹¹⁰ A. Sokolov,³² Y. Soloviev,¹⁰
E. Solovieva,^{48,58} S. Stanič,⁶⁹ M. Starič,³⁶ M. Steder,¹⁰ J. F. Strube,⁷³ J. Stypula,⁶⁶
S. Sugihara,¹⁰⁰ A. Sugiyama,⁸² M. Sumihama,¹⁴ K. Sumisawa,^{20,16} T. Sumiyoshi,¹⁰²
K. Suzuki,⁵⁹ K. Suzuki,⁸⁹ S. Suzuki,⁸² S. Y. Suzuki,²⁰ Z. Suzuki,⁹⁸ H. Takeichi,⁵⁹
M. Takizawa,^{86,21,80} U. Tamponi,^{34,104} M. Tanaka,^{20,16} S. Tanaka,^{20,16} K. Tanida,³⁵
N. Taniguchi,²⁰ G. N. Taylor,⁵⁴ F. Tenchini,⁵⁴ Y. Teramoto,⁷¹ I. Tikhomirov,⁵⁷

K. Trabelsi,^{20, 16} V. Trusov,³⁸ Y. F. Tse,⁵⁴ T. Tsuboyama,^{20, 16} M. Uchida,¹⁰¹ T. Uchida,²⁰
 S. Uehara,^{20, 16} K. Ueno,⁶⁵ T. Uglov,^{48, 58} Y. Unno,¹⁸ S. Uno,^{20, 16} S. Uozumi,⁴⁶ P. Urquijo,⁵⁴
 Y. Ushiroda,^{20, 16} Y. Usov,^{5, 70} S. E. Vahsen,¹⁹ C. Van Hulse,² P. Vanhoefer,⁵³ G. Varner,¹⁹
 K. E. Varvell,⁹¹ K. Vervink,⁴⁷ A. Vinokurova,^{5, 70} V. Vorobyev,^{5, 70} A. Vossen,²⁹
 M. N. Wagner,¹³ E. Waheed,⁵⁴ C. H. Wang,⁶⁴ J. Wang,⁷⁵ M.-Z. Wang,⁶⁵ P. Wang,³⁰
 X. L. Wang,^{73, 20} M. Watanabe,⁶⁸ Y. Watanabe,³⁷ R. Wedd,⁵⁴ S. Wehle,¹⁰ E. White,⁹
 E. Widmann,⁸⁹ J. Wiechczynski,⁶⁶ K. M. Williams,¹⁰⁷ E. Won,⁴⁴ B. D. Yabsley,⁹¹
 S. Yamada,²⁰ H. Yamamoto,⁹⁸ J. Yamaoka,⁷³ Y. Yamashita,⁶⁷ M. Yamauchi,^{20, 16}
 S. Yashchenko,¹⁰ H. Ye,¹⁰ J. Yelton,¹¹ Y. Yook,¹¹⁰ C. Z. Yuan,³⁰ Y. Yusa,⁶⁸ C. C. Zhang,³⁰
 L. M. Zhang,⁸³ Z. P. Zhang,⁸³ L. Zhao,⁸³ V. Zhilich,^{5, 70} V. Zhukova,⁵⁷ V. Zhulanov,^{5, 70}
 M. Ziegler,³⁸ T. Zivko,³⁶ A. Zupanc,^{49, 36} N. Zwahlen,⁴⁷ and O. Zyukova^{5, 70}

(The Belle Collaboration)

¹*Aligarh Muslim University, Aligarh 202002*

²*University of the Basque Country UPV/EHU, 48080 Bilbao*

³*Beihang University, Beijing 100191*

⁴*University of Bonn, 53115 Bonn*

⁵*Budker Institute of Nuclear Physics SB RAS, Novosibirsk 630090*

⁶*Faculty of Mathematics and Physics, Charles University, 121 16 Prague*

⁷*Chiba University, Chiba 263-8522*

⁸*Chonnam National University, Kwangju 660-701*

⁹*University of Cincinnati, Cincinnati, Ohio 45221*

¹⁰*Deutsches Elektronen-Synchrotron, 22607 Hamburg*

¹¹*University of Florida, Gainesville, Florida 32611*

¹²*Department of Physics, Fu Jen Catholic University, Taipei 24205*

¹³*Justus-Liebig-Universität Gießen, 35392 Gießen*

¹⁴*Gifu University, Gifu 501-1193*

¹⁵*II. Physikalisches Institut, Georg-August-Universität Göttingen, 37073 Göttingen*

¹⁶*SOKENDAI (The Graduate University for Advanced Studies), Hayama 240-0193*

¹⁷*Gyeongsang National University, Chinju 660-701*

¹⁸*Hanyang University, Seoul 133-791*

¹⁹*University of Hawaii, Honolulu, Hawaii 96822*

²⁰*High Energy Accelerator Research Organization (KEK), Tsukuba 305-0801*

²¹*J-PARC Branch, KEK Theory Center,*

High Energy Accelerator Research Organization (KEK), Tsukuba 305-0801

²²*Hiroshima Institute of Technology, Hiroshima 731-5193*

- ²³*IKERBASQUE, Basque Foundation for Science, 48013 Bilbao*
- ²⁴*University of Illinois at Urbana-Champaign, Urbana, Illinois 61801*
- ²⁵*Indian Institute of Science Education and Research Mohali, SAS Nagar, 140306*
- ²⁶*Indian Institute of Technology Bhubaneswar, Satya Nagar 751007*
- ²⁷*Indian Institute of Technology Guwahati, Assam 781039*
- ²⁸*Indian Institute of Technology Madras, Chennai 600036*
- ²⁹*Indiana University, Bloomington, Indiana 47408*
- ³⁰*Institute of High Energy Physics,
Chinese Academy of Sciences, Beijing 100049*
- ³¹*Institute of High Energy Physics, Vienna 1050*
- ³²*Institute for High Energy Physics, Protvino 142281*
- ³³*Institute of Mathematical Sciences, Chennai 600113*
- ³⁴*INFN - Sezione di Torino, 10125 Torino*
- ³⁵*Advanced Science Research Center,
Japan Atomic Energy Agency, Naka 319-1195*
- ³⁶*J. Stefan Institute, 1000 Ljubljana*
- ³⁷*Kanagawa University, Yokohama 221-8686*
- ³⁸*Institut für Experimentelle Kernphysik,
Karlsruher Institut für Technologie, 76131 Karlsruhe*
- ³⁹*Kavli Institute for the Physics and Mathematics of the Universe (WPI),
University of Tokyo, Kashiwa 277-8583*
- ⁴⁰*Kennesaw State University, Kennesaw, Georgia 30144*
- ⁴¹*King Abdulaziz City for Science and Technology, Riyadh 11442*
- ⁴²*Department of Physics, Faculty of Science,
King Abdulaziz University, Jeddah 21589*
- ⁴³*Korea Institute of Science and Technology Information, Daejeon 305-806*
- ⁴⁴*Korea University, Seoul 136-713*
- ⁴⁵*Kyoto University, Kyoto 606-8502*
- ⁴⁶*Kyungpook National University, Daegu 702-701*
- ⁴⁷*École Polytechnique Fédérale de Lausanne (EPFL), Lausanne 1015*
- ⁴⁸*P.N. Lebedev Physical Institute of the Russian Academy of Sciences, Moscow 119991*
- ⁴⁹*Faculty of Mathematics and Physics,
University of Ljubljana, 1000 Ljubljana*
- ⁵⁰*Ludwig Maximilians University, 80539 Munich*
- ⁵¹*Luther College, Decorah, Iowa 52101*
- ⁵²*University of Maribor, 2000 Maribor*
- ⁵³*Max-Planck-Institut für Physik, 80805 München*

- ⁵⁴School of Physics, University of Melbourne, Victoria 3010
⁵⁵Middle East Technical University, 06531 Ankara
⁵⁶University of Miyazaki, Miyazaki 889-2192
⁵⁷Moscow Physical Engineering Institute, Moscow 115409
⁵⁸Moscow Institute of Physics and Technology, Moscow Region 141700
⁵⁹Graduate School of Science, Nagoya University, Nagoya 464-8602
⁶⁰Kobayashi-Maskawa Institute, Nagoya University, Nagoya 464-8602
⁶¹Nara University of Education, Nara 630-8528
⁶²Nara Women's University, Nara 630-8506
⁶³National Central University, Chung-li 32054
⁶⁴National United University, Miao Li 36003
⁶⁵Department of Physics, National Taiwan University, Taipei 10617
⁶⁶H. Niewodniczanski Institute of Nuclear Physics, Krakow 31-342
⁶⁷Nippon Dental University, Niigata 951-8580
⁶⁸Niigata University, Niigata 950-2181
⁶⁹University of Nova Gorica, 5000 Nova Gorica
⁷⁰Novosibirsk State University, Novosibirsk 630090
⁷¹Osaka City University, Osaka 558-8585
⁷²Osaka University, Osaka 565-0871
⁷³Pacific Northwest National Laboratory, Richland, Washington 99352
⁷⁴Panjab University, Chandigarh 160014
⁷⁵Peking University, Beijing 100871
⁷⁶University of Pittsburgh, Pittsburgh, Pennsylvania 15260
⁷⁷Punjab Agricultural University, Ludhiana 141004
⁷⁸Research Center for Electron Photon Science,
Tohoku University, Sendai 980-8578
⁷⁹Research Center for Nuclear Physics, Osaka University, Osaka 567-0047
⁸⁰Theoretical Research Division, Nishina Center, RIKEN, Saitama 351-0198
⁸¹RIKEN BNL Research Center, Upton, New York 11973
⁸²Saga University, Saga 840-8502
⁸³University of Science and Technology of China, Hefei 230026
⁸⁴Seoul National University, Seoul 151-742
⁸⁵Shinshu University, Nagano 390-8621
⁸⁶Showa Pharmaceutical University, Tokyo 194-8543
⁸⁷Soongsil University, Seoul 156-743
⁸⁸University of South Carolina, Columbia, South Carolina 29208
⁸⁹Stefan Meyer Institute for Subatomic Physics, Vienna 1090

⁹⁰*Sungkyunkwan University, Suwon 440-746*

⁹¹*School of Physics, University of Sydney, New South Wales 2006*

⁹²*Department of Physics, Faculty of Science, University of Tabuk, Tabuk 71451*

⁹³*Tata Institute of Fundamental Research, Mumbai 400005*

⁹⁴*Excellence Cluster Universe, Technische Universität München, 85748 Garching*

⁹⁵*Department of Physics, Technische Universität München, 85748 Garching*

⁹⁶*Toho University, Funabashi 274-8510*

⁹⁷*Tohoku Gakuin University, Tagajo 985-8537*

⁹⁸*Department of Physics, Tohoku University, Sendai 980-8578*

⁹⁹*Earthquake Research Institute, University of Tokyo, Tokyo 113-0032*

¹⁰⁰*Department of Physics, University of Tokyo, Tokyo 113-0033*

¹⁰¹*Tokyo Institute of Technology, Tokyo 152-8550*

¹⁰²*Tokyo Metropolitan University, Tokyo 192-0397*

¹⁰³*Tokyo University of Agriculture and Technology, Tokyo 184-8588*

¹⁰⁴*University of Torino, 10124 Torino*

¹⁰⁵*Toyama National College of Maritime Technology, Toyama 933-0293*

¹⁰⁶*Utkal University, Bhubaneswar 751004*

¹⁰⁷*Virginia Polytechnic Institute and State University, Blacksburg, Virginia 24061*

¹⁰⁸*Wayne State University, Detroit, Michigan 48202*

¹⁰⁹*Yamagata University, Yamagata 990-8560*

¹¹⁰*Yonsei University, Seoul 120-749*

Abstract

We report results on the studies of the $e^+e^- \rightarrow B_s^{(*)}\bar{B}_s^{(*)}$ processes. The results are based on a 121.4 fb^{-1} data sample collected with the Belle detector at the center-of-mass energy near the $\Upsilon(10860)$ peak and 16.4 fb^{-1} of data collected at 19 energy points in the range from 10.77 to 11.02 GeV. We observe a clear $e^+e^- \rightarrow \Upsilon(10860) \rightarrow B_s^{(*)}\bar{B}_s^{(*)}$ signal, with no statistically significant signal of $e^+e^- \rightarrow \Upsilon(11020) \rightarrow B_s^{(*)}\bar{B}_s^{(*)}$. The relative production ratio of $B_s^*\bar{B}_s^*$, $B_s\bar{B}_s^*$, and $B_s\bar{B}_s$ final states at $\sqrt{s} = 10.866 \text{ GeV}$ is measured to be $7 : 0.856 \pm 0.106(\text{stat.}) \pm 0.053(\text{syst.}) : 0.645 \pm 0.094(\text{stat.})_{-0.033}^{+0.030}(\text{syst.})$. An angular analysis of the $B_s^*\bar{B}_s^*$ final state produced at the $\Upsilon(10860)$ peak is also performed.

PACS numbers: 14.40.Pq, 13.25.Gv, 12.39.Pu

INTRODUCTION

The Belle experiment has recently measured the ratio $R_b = \sigma_{e^+e^- \rightarrow b\bar{b}}/\sigma_{e^+e^- \rightarrow \mu^+\mu^-}$ in the energy range from 10.60 to 11.02 GeV utilizing an inclusive technique [1]. In addition, the energy dependence of the production cross section has been studied for several exclusive channels such as $e^+e^- \rightarrow \Upsilon(nS)\pi^+\pi^-$ ($n = 1, 2, 3$) [1] and $e^+e^- \rightarrow h_b(mP)\pi^+\pi^-$ ($m = 1, 2$) [2]. The measured energy dependence for the aforementioned exclusive cross sections exhibits substantially different behaviour compared to that for R_b . Measurements of the cross sections for other exclusive final states, such as two-body $B^{(*)}\bar{B}^{(*)}$, $B_s^{(*)}\bar{B}_s^{(*)}$, and three-body $B^{(*)}\bar{B}^{(*)}\pi$, might shed light on the mechanisms of the $b\bar{b}$ hadronization and on the nature of the $\Upsilon(10860)$ and $\Upsilon(11020)$ resonances.

In this paper, we present preliminary results on the analysis of the $e^+e^- \rightarrow B_s^{(*)}\bar{B}_s^{(*)}$ processes in the energy range from 10.77 to 11.02 GeV in the center-of-mass (c.m.) frame using data accumulated with the Belle detector [3] operating at the asymmetric-energy e^+e^- collider KEKB [4].

THE BELLE DETECTOR

The Belle detector is a large-solid-angle magnetic spectrometer based on a 1.5 T superconducting solenoid magnet. Charged particle tracking is provided by a four-layer silicon vertex detector and a 50-layer central drift chamber (CDC) that surround the interaction point. The charged particle acceptance covers laboratory polar angle θ between 17° and 150° , corresponding to about 92% of the total solid angle in the c.m. frame.

Charged hadron identification is provided by dE/dx measurements in the CDC, an array of 1188 aerogel Cherenkov counters (ACC), and a barrel-like array of 128 time-of-flight scintillation counters (TOF); information from the three subdetectors is combined to form a single likelihood ratio, which is then used in kaon and pion selection. Electromagnetic showering particles are detected in an array of 8736 CsI(Tl) crystals (ECL) that covers nearly the same solid angle as the charged particle tracking system.

Electron identification in Belle is based on a combination of dE/dx measurements in the CDC, the response of the ACC, and the position, shape and total energy deposition of the shower detected in the ECL. The electron identification efficiency is greater than 92% for tracks with $p_{\text{lab}} > 1.0$ GeV/ c and the hadron misidentification probability is below 0.3%. The magnetic field is returned via an iron yoke that is instrumented to detect muons and K_L^0 mesons. Muons are identified based on their penetration range and transverse scattering in this KLM detector. In the momentum region relevant to this analysis, the identification efficiency is about 90% while the probability to misidentify a pion as a muon is below 2%.

We use the EvtGen event generator [5] with PHOTOS [6] for radiative corrections and a GEANT-based Monte Carlo (MC) simulation [7] to model the response of the detector and determine the acceptance. The MC simulation includes run-dependent detector performance variations and background conditions.

EVENT RECONSTRUCTION

Charged tracks are selected with a set of track quality requirements based on the number of CDC hits and on the distances of closest approach to the interaction point (IP) along (perpendicular to) the beam axis of $|dz| < 5$ cm ($(dr) < 2.5$ cm). Tracks originating from a B_s candidate are required to have momenta transverse to the beam greater than 0.05 GeV/ c . For charged kaon identification, we impose a particle-identification requirement that has an 86% efficiency and a 7% fake rate from misidentified pions. Charged hadron candidates that are positively identified as electrons are excluded.

B_s Reconstruction

Candidate B_s decays are reconstructed in the following channels: $B_s \rightarrow D_s^{(*)-}\pi^+$, $B_s \rightarrow J/\psi K^+K^-$, $B_s \rightarrow J/\psi\pi^+\pi^-$, and $B_s \rightarrow \psi(2S)K^+K^-$. Candidate D_s^* decays are reconstructed in the $D_s\gamma$ channel, where $D_s \rightarrow K^+K^-\pi^-$ or $K_S^0K^-$. D_s candidates from the $B_s \rightarrow D_s^-\pi^+$ decay mode are reconstructed in the $K^+K^-\pi^-$, $K_S^0K^-$, and $K_S^0K^+\pi^-\pi^-$ final states. Neutral kaon (K_S^0) candidates are reconstructed using pairs of oppositely-charged tracks, both treated as pions, with an invariant mass within 15 MeV/ c^2 of the nominal K_S^0 mass; the IP constraint is not imposed here. The direction of the K_S^0 candidate momentum vector is required to be consistent with the direction of its vertex displacement relative to the IP. To identify signal D_s [D_s^*] candidates, we require $|M(D_s) - m_{D_s}| < 2.5\sigma$ [$|(M(D_s\gamma) - M(D_s)) - (m_{D_s^*} - m_{D_s})| < 2.5\sigma$], where m_{D_s} [$m_{D_s^*}$] is the D_s [D_s^*] nominal mass [8], and σ is the Gaussian width for the relevant final state. The invariant mass of the $J/\psi \rightarrow \ell^+\ell^-$ candidates, with ℓ being electron (muon), is required to satisfy 3.01 (3.05) GeV/ $c^2 < M(\ell^+\ell^-) < 3.13$ GeV/ c^2 . The $\psi(2S)$ candidates are reconstructed in the $\psi(2S) \rightarrow J/\psi\pi^+\pi^-$ decay mode. We require $|(M(J/\psi\pi^+\pi^-) - M(J/\psi)) - (m_{\psi(2S)} - m_{J/\psi})| < 8$ MeV/ c^2 , where $m_{J/\psi}$ and $m_{\psi(2S)}$ are the J/ψ and $\psi(2S)$ nominal masses [8], respectively.

We identify B_s candidates by their reconstructed invariant mass $M(B_s)$ and momentum $P(B_s)$. We do not reconstruct the photon from the $B_s^* \rightarrow B_s\gamma$ decay; instead, the individual two-body final states are discriminated based on the reconstructed B_s momentum.

Signal $\Upsilon(10860) \rightarrow B_s^* \bar{B}_s^*$ events produce a narrow peak in the $P(B_s)$ spectrum around 0.442 GeV/ c , the $\Upsilon(10860) \rightarrow B_s \bar{B}_s^*$ signal events produce a peak at 0.678 GeV/ c , and $\Upsilon(10860) \rightarrow B_s \bar{B}_s$ signal peaks at 0.844 GeV/ c . It is important to note here that, due to the very low momentum of the photon from the $B_s^* \rightarrow B_s \gamma$ decays, the $B_s \bar{B}_s^*$ events (where the reconstructed B_s is the one from B_s^*) produce a peak in the $P(B_s)$ distribution at about the same position as $B_s \bar{B}_s^*$ events, where the reconstructed B_s is the prompt one. This is confirmed with the signal MC simulation. Momentum smearing for B_s daughters from B_s^* decays becomes more significant for higher E_{cm} values.

Background Suppression

The dominant source of background arises from $e^+e^- \rightarrow c\bar{c}$ continuum events, where real D mesons produced in e^+e^- annihilation are combined with random particles to form a B candidate. This type of background is suppressed using variables that characterize the event topology. Since the momenta of the $B_s^{(*)}$ and $\bar{B}_s^{(*)}$ mesons produced from the $\Upsilon(10860)$ decay are low in the c.m. frame, their decay products are essentially uncorrelated and the event tends to be spherical. In contrast, hadrons from continuum events tend to exhibit a two-jet structure. We use θ_{thr} , the angle between the thrust axis [9] of the B_s candidate and that of the rest of the event, to discriminate between the two cases. The distribution is strongly peaked near $|\cos \theta_{\text{thr}}| = 1.0$ for $q\bar{q}$ events and is nearly flat in $\cos \theta_{\text{thr}}$ for $B_s^{(*)} \bar{B}_s^{(*)}$ events. We require $|\cos \theta_{\text{thr}}| < 0.80$ for the $B_s \rightarrow D_s^{(*)}\pi$ final states; this eliminates about 83% of the continuum background and retains 79% of the signal events.

ANALYSIS OF THE $\Upsilon(10860)$ DATA

Figures 1(a), (b), and (c) show the combined $M(B_s)$ distribution for the generic $\Upsilon(10860) \rightarrow B^{(*)} \bar{B}^{(*)}$ MC, generic $\Upsilon(10860) \rightarrow B_s^{(*)} \bar{B}_s^{(*)}$ MC (with signal modes removed), and continuum $\Upsilon(10860) \rightarrow q\bar{q}$ ($q = u, d, s, c$) MC, respectively, with a requirement on the B_s candidate momentum of $P(B_s) < 0.95$ GeV/ c .

The combined $M(B_s)$ distribution for the selected B_s candidates in data is shown in Fig. 1(d). To determine the B_s signal yield, we perform a binned maximum likelihood fit of the $M(B_s)$ distribution to the non-coherent sum of signal and background components. The signal is parametrized by the sum of two Gaussian functions with a common mean, a ratio of widths fixed from the signal MC at $\sigma_2 = 2.1\sigma_1$, and a relative area of $N_2 = 0.36N_1$. The background component is comprised of the continuum background and the B - and B_s -related background. As evident from Figs. 1(a) and (c), the B -related and continuum backgrounds

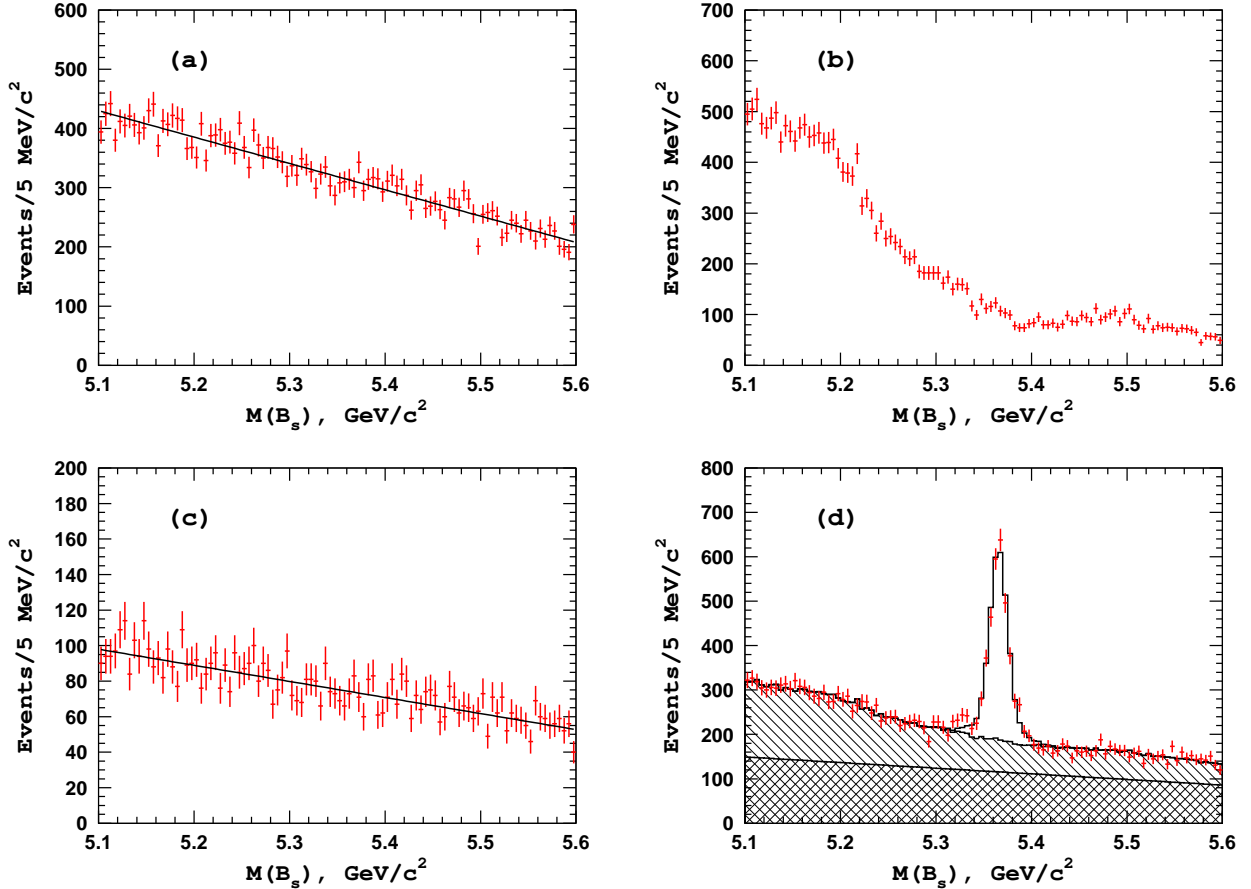


FIG. 1: Mass distribution for the selected B_s candidates (all modes combined) in the (a) B_u and B_d generic MC, (b) B_s generic MC except for signal modes, (c) continuum $e^+e^- \rightarrow q\bar{q}$ generic MC, and (d) $\Upsilon(10860)$ data. The black histogram in (d) represents result of the fit with the signal component shown by the open histogram, B - and B_s -related background by the hatched histogram, and the continuum background by the cross-hatched histogram.

are featureless, so we parametrize these by linear functions. The shape of the B_s -related background, shown in Fig. 1(b), is fixed from the generic MC, while the normalization is fixed to be a fraction of the observed B_s signal. The ratio of the number of the background events due to other B_s decays to the number of events in the B_s peak is determined to be 1.87 for the $P(B_s)$ requirement used to select a combination of $B_s^{(*)}\bar{B}_s^{(*)}$ final states and 1.12 for the $B_s^*\bar{B}_s^*$ final state. If the normalization is allowed to float while fitting the data, the fits yield 1.82 ± 0.22 and 1.06 ± 0.13 , respectively. The result of the fit to the $M(B_s)$ distribution is shown in Fig. 1(d). The fit yields 2283 ± 63 signal B_s decays.

To distinguish between individual two-body $e^+e^- \rightarrow B_s^{(*)}\bar{B}_s^{(*)}$ processes, we impose a requirement on the invariant mass of the B_s candidate equivalent to a Gaussian 2.5σ efficiency, where σ is a B_s decay mode-dependent parameter. Figures 2(a), (b), and (c) show the

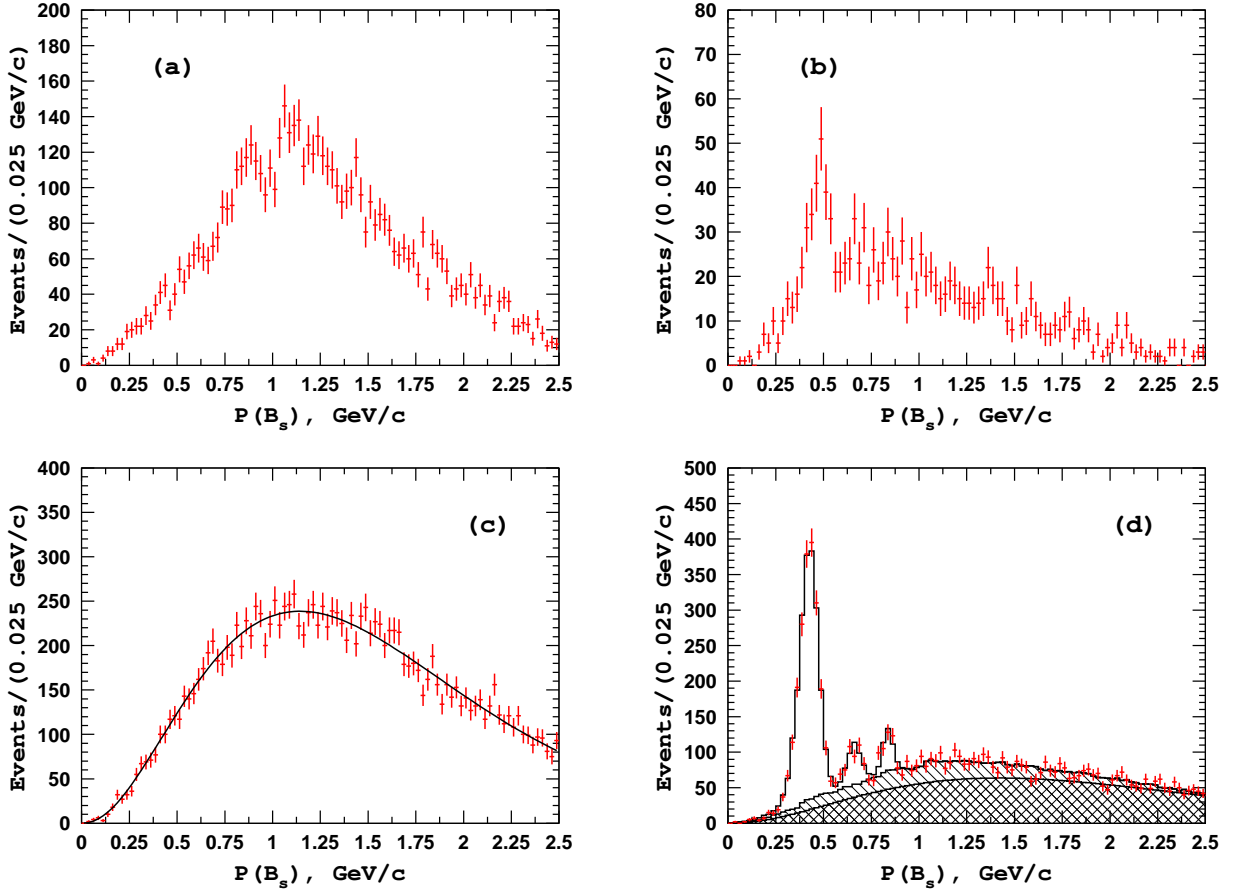


FIG. 2: Momentum distribution for the selected B_s candidates (all modes combined) in the (a) B_u and B_d generic MC, (b) B_s generic MC with signal modes removed, (c) continuum $e^+e^- \rightarrow q\bar{q}$ generic MC, and (d) $\Upsilon(10860)$ data. The black histogram in (d) represents a result of the fit with the signal component shown by the open histogram, B - and B_s -related background by the hatched histogram, and the continuum background by the cross-hatched histogram.

$P(B_s)$ distribution for the generic $\Upsilon(10860) \rightarrow B^{(*)}\bar{B}^{(*)}$ MC, generic $\Upsilon(10860) \rightarrow B_s^{(*)}\bar{B}_s^{(*)}$ MC (with signal modes removed), and continuum $\Upsilon(10860) \rightarrow q\bar{q}$ MC, respectively, with a B_s decay mode-dependent requirement on the $M(B_s)$ that corresponds to a Gaussian 2.5σ efficiency. A peaking structure observed in Fig. 2(b) around $P(B_s) \sim 0.5$ GeV/c is due to misreconstructed B_s candidates, such as $B_s^0 \rightarrow D_s^-\pi^+$, $D_s^- \rightarrow K^+K^-\pi^-$ with double π/K misidentification. Such events produce no peak in the $M(B_s)$ distribution but do peak in $P(B_s)$. The momentum distribution for the selected B_s candidates in data is shown in Fig. 2(d). Three distinct peaks, corresponding to the $B_s\bar{B}_s$, $B_s\bar{B}_s^* + \bar{B}_sB_s^*$, and $B_s^*\bar{B}_s^*$ final states, are apparent.

We perform a binned maximum likelihood fit of the $P(B_s)$ distribution to the non-

coherent sum of three signal components and a background component. The shape of each signal component is determined from MC simulation with the initial state radiation (ISR) effect taken into account. The background component is comprised of the continuum background, the B -related background, and the B_s -related background. The shape of the continuum $P(B_s)$ background is parametrized as

$$B_{qq}(x) \sim x^\alpha e^{-(x/x_0)^\beta}, \quad (1)$$

where $x = P(B_s)$; x_0 , α , and β are fit parameters. The normalization of the continuum background component is allowed to float. For the B - and B_s -related background components, we use the corresponding MC driven histograms (see Fig. 2) as PDFs. The ratios of the B - and B_s -related backgrounds to the $B_s^{(*)}$ signal yield are fixed from the MC simulation.

Results of the fit to the $P(B_s)$ distribution are shown in Fig. 2(d). The fit yields 1854 ± 51 $B_s^* \bar{B}_s^*$ signal events, 226 ± 27 $B_s \bar{B}_s^* + \bar{B}_s B_s^*$ signal events, and 169 ± 24 $B_s \bar{B}_s$ signal events. Assuming a uniform reconstruction efficiency over the relevant B_s momentum range, this corresponds to relative fractions of $7 : 0.853 \pm 0.106(\text{stat.}) \pm 0.053(\text{syst.}) : 0.638 \pm 0.094(\text{stat.}) \pm 0.033(\text{syst.})$. These can be compared with the current world average results of $7 : 0.537 \pm 0.152 : 0.199 \pm 0.199$ [8] and an expectation of $7 : 4 : 1$ in the heavy-quark spin symmetry (HQSS) approximation [10, 11].

The dominant sources of the systematic uncertainties for the relative fractions of the two-body signals are:

- the fraction of the B - and B_s -related background estimating by repeating the fit to the B_s momentum distribution with the normalization of this background allowed to float;
- the $M(B_s)$ signal region, estimated by repeating the fit to the data with the $M(B_s)$ signal region set to $\pm 3\sigma$ and $\pm 2\sigma$ around the B_s nominal mass;
- the momentum distribution fitting range, estimated by varying the upper boundary of the momentum range from 2.0 to 3.0 GeV/ c with a 0.25 GeV/ c step;
- the width of the momentum resolution function, estimated by varying the width of the $P(B_s)$ resolution within $\pm 10\%$ of the nominal value and repeating the fit to the data.

These uncertainties are summarized in Table I. The overall systematic uncertainty is estimated to be ± 0.053 for the $B_s \bar{B}_s^* + \bar{B}_s B_s^*$ fraction and ± 0.033 for the $B_s \bar{B}_s$ fraction.

TABLE I: Summary of the systematic studies for the relative $B_s^*\bar{B}_s^* : B_s\bar{B}_s^* + \bar{B}_sB_s^* : B_s\bar{B}_s$ yields.

Source	Signal yield, events			Ratio	Uncertainty
	$B_s^*\bar{B}_s^*$	$B_s\bar{B}_s^*$	$B_s\bar{B}_s$		
$B\&B_s$ background					
floating	1865	219	168	7 : 0.822 : 0.637	
$\times 1.50$	1844	227	164	7 : 0.862 : 0.623	
$\times 0.75$	1863	221	172	7 : 0.830 : 0.646	
					$+0.009 \quad +0.008$ $-0.021 \quad -0.015$
$M(B_s)$ signal region					
$\pm 2\sigma$	1780	212	162	7 : 0.834 : 0.637	
$\pm 3\sigma$	1897	235	174	7 : 0.867 : 0.642	
					$+0.014 \quad +0.004$ $-0.019 \quad -0.001$
$P(B_s)$ range					
$< 2.00 \text{ GeV}/c$	1864	226	165	7 : 0.851 : 0.626	
$< 2.25 \text{ GeV}/c$	1857	225	167	7 : 0.851 : 0.636	
$< 2.75 \text{ GeV}/c$	1859	222	165	7 : 0.838 : 0.628	
$< 3.00 \text{ GeV}/c$	1871	231	173	7 : 0.871 : 0.647	
					$+0.018 \quad +0.005$ $-0.015 \quad -0.016$
Momentum resolution					
$B_s^*\bar{B}_s^* : -10\%$	1842	213	162	7 : 0.811 : 0.622	
$B_s^*\bar{B}_s^* : +10\%$	1865	239	177	7 : 0.900 : 0.671	
$B_s\bar{B}_s^* : -10\%$	1855	226	169	7 : 0.855 : 0.644	
$B_s\bar{B}_s^* : +10\%$	1856	218	162	7 : 0.824 : 0.617	
$B_s\bar{B}_s : -10\%$	1854	227	171	7 : 0.860 : 0.652	
$B_s\bar{B}_s : +10\%$	1854	224	166	7 : 0.848 : 0.633	
					$+0.047 \quad +0.029$ $-0.042 \quad -0.025$
Nominal fit	1854 ± 51	226 ± 27	169 ± 24	$7 : 0.853 \pm 0.106 : 0.638 \pm 0.094$	$+0.053 \quad +0.030$ $-0.053 \quad -0.033$

B_s reconstruction efficiency

To account for the possible dependence of the B_s reconstruction efficiency on the c.m. energy ($P(B_s)$ momentum), we generate 20K $e^+e^- \rightarrow B_s^{(*)}\bar{B}_s^{(*)}$ signal MC events at seven E_{cm} points. Applying the same reconstruction and analysis algorithm, we determine the B_s signal yield. The results are summarized in Fig. 3. No significant variations in the reconstruction efficiency are observed within the relevant B_s momentum range, including the case where the $\cos(\theta_{\text{thr}})$ requirement is applied.

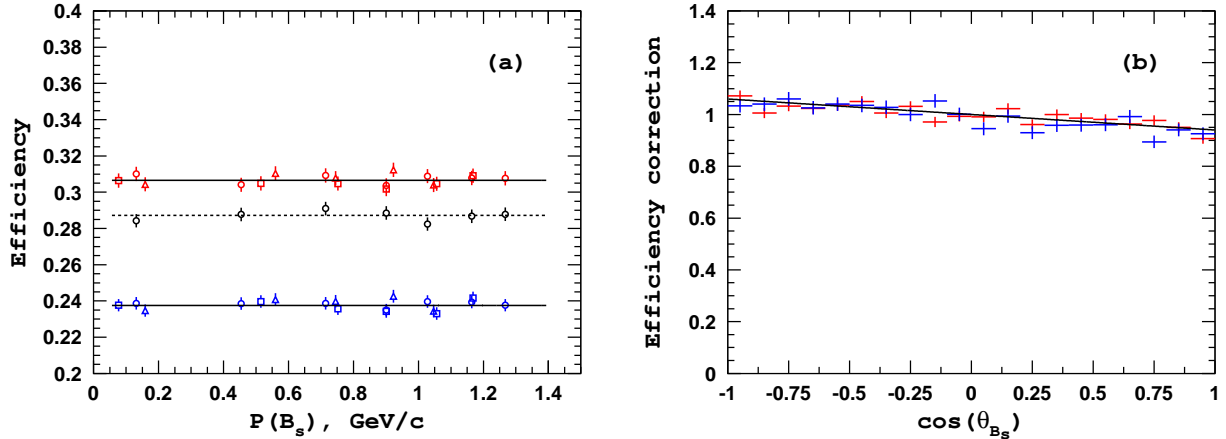


FIG. 3: B_s reconstruction efficiency (no intermediate branching fractions included). (a) Momentum dependence of the B_s reconstruction efficiency for the $B_s \rightarrow D_s[K^+K^-\pi]\pi$ decay mode with no $\cos(\theta_{\text{thr}})$ cut (red points), with the $|\cos(\theta_{\text{thr}})| < 0.8$ cut applied (blue points), and for the $B_s \rightarrow J/\psi[\ell^+\ell^-]K^+K^-$ decay mode (black points). (b) Correction for the B_s reconstruction efficiency as a function of the B_s polar angle in the c.m. frame. Red points are for the $B_s \rightarrow D_s[K^+K^-\pi]\pi$ decay mode, blue points are for the $B_s \rightarrow J/\psi[\mu^+\mu^-]K^+K^-$ decay mode. The solid line represents the result of the fit to a linear function.

Angular analysis

The $\cos(\theta_{B_s^*})$ distribution, where $\theta_{B_s^*}$ is the angle between the B_s^* momentum and the z axis in the c.m. frame, provides information on the relative fractions of the $S = 0$ and $S = 2$ states, with S being the total spin of the $B_s^*\bar{B}_s^*$ pair, produced in the $e^+e^- \rightarrow B_s^*\bar{B}_s^*$ process. The angular distribution of the $S = 0$ component is proportional to $1 - \cos^2(\theta_{B_s^*})$ while that for the $S = 2$ component to $(7 - \cos^2(\theta_{B_s^*}))/10$. The differential cross section then reads as

$$\frac{d\sigma}{d\cos(\theta_{B_s^*})} \sim \mathcal{A}_0^2 + \mathcal{A}_2^2, \quad (2)$$

where $\mathcal{A}_0^2 = a_0^2(1 - \cos^2 \theta_{B_s^*})$ and $\mathcal{A}_2^2 = a_2^2(7 - \cos^2 \theta_{B_s^*})/10$ are the squared amplitudes for the $B_s^*\bar{B}_s^*$ production in a P wave with the total spin of $S = 0$ and $S = 2$, respectively. In the heavy quark spin symmetry, the ratio $a_0^2 : a_2^2$ is expected to be 1:20. However, the proximity of the $B_s^*\bar{B}_s^*$ production threshold might distort this ratio significantly [12].

For the analysis of the B_s^* polar angular distribution in data, we select B_s^* candidates by applying a requirement on the B_s momentum of $0.25 \text{ GeV}/c < P(B_s) < 0.55 \text{ GeV}/c$ and then determine the B_s yield in $\cos(\theta_{B_s})$ bins. (In fact, we measure the polar angle of the B_s meson, not B_s^* . The associated absolute uncertainty in $\cos \theta_{B_s^*}$ is below 0.01, which is much smaller than the bin width.) We perform a binned maximum likelihood fit to the $M(B_s)$

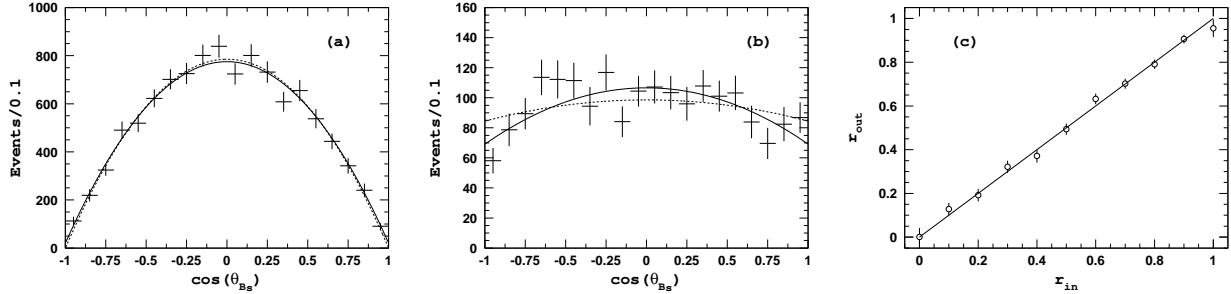


FIG. 4: $\cos(\theta_{B_s})$ distribution for the $e^+e^- \rightarrow B_s^*\bar{B}_s^*$ events. (a) Test with generic MC events. The solid line – a fit with combinations of the $S = 0$ and $S = 2$ components; the dashed line – a fit with the $S = 0$ component only. (b) $\Upsilon(10860)$ data. Th solid line – a fit with combinations of the $S = 0$ and $S = 2$ components; the dashed line – fit with the $S = 2$ component only. (c) measured r value versus the input one as determined with signal MC; the solid line shows the exact proportionality.

distribution for each $\cos \theta_{B_s}$ bin. The B_s yield as a function of $\cos \theta_{B_s}$ is fit to the following function:

$$\frac{d\sigma}{d \cos(\theta_{B_s})} \sim r(1 - \cos^2 \theta_{B_s}) + (1 - r)\frac{7 - \cos^2 \theta_{B_s}}{10}, \quad (3)$$

where $r = a_0^2/(a_2^2 + a_0^2)$. We also apply the efficiency corrections described earlier.

As a cross-check of the analysis procedure, we apply it to the generic MC events. Results of this analysis are shown in Fig. 4(a). The fit result of $r = 0.952 \pm 0.029$ is consistent with a pure $S = 0$ component. This agrees with the MC input, where the fraction of the $S = 2$ component is (wrongly) set to zero.

Results of the same analysis applied to the data are shown in Fig. 4(b). The fit yields a fraction of the $S = 0$ component of $r = 0.175 \pm 0.057^{+0.022}_{-0.018}$. We also fit the data with a pure $S = 2$ form, the results are also shown in Fig. 4(b). The statistical significance of the $S = 0$ component, determined as $\sqrt{-2(\ln \mathcal{L}_{S=2} - \ln \mathcal{L}_{\text{mix}})}$ is 3.1 standard deviations (statistical only).

The dominant sources of the systematic uncertainties for the angular analysis are

- correction for the reconstruction efficiency – $^{+0.004}_{-0.000}$: to estimate this uncertainty, we vary the slope of the correction function within its statistical uncertainty;
- binning – ± 0.010 : to estimate this uncertainty, we repeat the fit with bin widths of 0.040, 0.050, 0.080, 0.125, and 0.200, then take the largest positive and negative deviations as the estimation of the systematic uncertainty;
- determination of the B_s signal yield – $^{+0.015}_{-0.008}$: here, we vary the fraction of the B_s related component within $\pm 25\%$ and fraction of the second Gaussian in the signal PDF within

$\pm 10\%$ (the typical variation of these quantities for various B_s decay chains) and repeat the fit to the angular distribution;

- momentum cuts to select the $B_s^* \bar{B}_s^*$ signal – ± 0.012 : here, we vary the lower and the higher boundary of the momentum range by ± 0.05 GeV/ c and repeat the fit to the angular distribution.

We also check for a possible systematic shift in the determination of the r value (linearity check) using signal MC events generated with various inputs for the $S = 0$ fraction. The results of this study are shown in Fig. 4(c).

The overall systematic uncertainty is calculated as the quadratic sum of all contributions and is $^{+0.022}_{-0.018}$. This reduces the significance of the $S = 0$ component to 2.6σ .

ANALYSIS OF THE ENERGY SCAN DATA

For this analysis, we use 19 energy points above the $B_s B_s$ production threshold with about one inverse femtobarn of integrated luminosity accumulated at each point. We also split the 121.4 fb $^{-1}$ of data taken near the $\Upsilon(10860)$ peak into three samples with close E_{cm} values according to the KEKB data; see Table II.

At each energy point, we use the same analysis strategy as applied in the analysis of the $\Upsilon(10860)$ data, described in the previous Section. The $M(B_s)$ distributions for selected B_s candidates at each energy point are shown in Fig 5. The relevant information is summarized in Table II.

The visible cross section σ^{vis} shown in Fig. 6(a) is calculated as

$$\sigma_i^{\text{vis}} = 0.0585 \frac{N_i}{N_{5S}} \frac{L_{5S}}{L_i}, \quad (4)$$

where N_i and $N_{5S} = 2270 \pm 60$ are the B_s yields measured at the i -th energy point and for the full $\Upsilon(10860)$ sample, respectively; L_i and $L_{5S} = 121.4$ fb $^{-1}$ are the corresponding luminosities. The factor (0.0585 ± 0.0106) nb is the product of the total $e^+e^- \rightarrow b\bar{b}$ cross section of 0.340 ± 0.016 nb [13] and the fraction of $e^+e^- \rightarrow b\bar{b}$ events hadronized to a pair of $B_s^{(*)}$ mesons, measured to be $f_s = 0.172 \pm 0.030$ [13]. Both these quantities have been measured by Belle at the $\Upsilon(10860)$.

In addition to the total $e^+e^- \rightarrow B_s^{(*)} \bar{B}_s^{(*)}$ cross section, we also perform a separate measurement of the exclusive $e^+e^- \rightarrow B_s^* \bar{B}_s^*$ cross section. We select $B_s^* \bar{B}_s^*$ events by applying a tighter requirement on the momentum of the reconstructed B_s , as summarized in Table II. Results are presented in Fig. 6(b) and in Table II. As a cross check, we apply the same procedure to events selected in a 0.25 GeV/ c -wide momentum window above the two-body

TABLE II: Summary of the energy scan results.

#	Energy	Lumi.	Total $B_s^{(*)}\bar{B}_s^{(*)}$			Only $B_s^*\bar{B}_s^*$		
			$P(B_s)$	B_s Yield (Events)	σ_{vis} (pb)	$P(B_s)$	B_s Yield (Events)	σ_{vis} (pb)
(GeV)	(fb $^{-1}$)	(GeV/c)				(GeV/c)		
1	10.7711	0.955	< 0.605	3.0 ± 2.3	$9.8 \pm 7.5 \pm 3.2$	—	—	—
2	10.8205	1.697	< 0.793	4.8 ± 4.1	$8.8 \pm 7.5 \pm 2.9$	—	—	—
3	10.8497	0.989	< 0.888	14.3 ± 6.2	$45.0 \pm 19.5 \pm 8.7$	< 0.461	12.3 ± 3.3	$38.7 \pm 10.4 \pm 7.2$
4	10.8589	0.988	< 0.916	26.8 ± 6.3	$84.4 \pm 19.9 \pm 15.7$	< 0.520	15.8 ± 3.4	$49.8 \pm 10.7 \pm 9.3$
5	10.8695	0.978	< 0.947	28.6 ± 6.2	$91.0 \pm 19.7 \pm 17.2$	< 0.578	20.6 ± 3.9	$65.6 \pm 12.4 \pm 12.2$
6	10.8785	0.978	< 0.973	13.5 ± 5.4	$43.0 \pm 17.2 \pm 8.3$	< 0.622	12.3 ± 3.9	$39.2 \pm 12.4 \pm 7.3$
7	10.8836	1.848	< 0.987	24.5 ± 7.1	$41.3 \pm 12.0 \pm 7.7$	< 0.644	20.5 ± 5.8	$34.5 \pm 9.8 \pm 6.4$
8	10.8889	0.990	< 1.003	10.1 ± 5.1	$31.8 \pm 16.0 \pm 6.0$	< 0.668	4.3 ± 2.8	$13.5 \pm 8.8 \pm 4.5$
9	10.8985	0.983	< 1.029	11.2 ± 4.7	$35.5 \pm 14.9 \pm 6.6$	< 0.708	3.3 ± 2.8	$10.5 \pm 8.9 \pm 3.5$
10	10.9011	1.425	< 1.036	13.7 ± 4.9	$30.0 \pm 10.7 \pm 5.8$	< 0.718	9.8 ± 4.0	$21.4 \pm 8.7 \pm 5.3$
11	10.9077	0.980	< 1.053	-2.8 ± 3.8	$-8.9 \pm 12.1 \pm 4.1$	< 0.744	-1.1 ± 3.5	$-3.5 \pm 11.1 \pm 2.6$
12	10.9275	1.149	< 1.105	5.6 ± 4.8	$12.1 \pm 13.0 \pm 4.3$	< 0.815	4.4 ± 3.4	$11.9 \pm 9.2 \pm 4.2$
13	10.9575	0.969	< 1.178	-0.2 ± 3.6	$-0.6 \pm 11.6 \pm 2.3$	< 0.912	2.3 ± 3.3	$7.4 \pm 10.1 \pm 3.4$
14	10.9775	0.999	< 1.224	2.9 ± 4.7	$9.0 \pm 14.6 \pm 3.3$	< 0.971	2.8 ± 3.2	$8.7 \pm 10.0 \pm 3.2$
15	10.9919	0.985	< 1.258	-4.5 ± 3.3	$-14.2 \pm 10.4 \pm 4.1$	< 1.012	-1.0 ± 2.6	$-3.1 \pm 8.2 \pm 2.5$
16	11.0068	0.976	< 1.290	-2.9 ± 4.2	$-9.3 \pm 13.4 \pm 3.8$	< 1.052	-3.5 ± 2.7	$-11.2 \pm 8.6 \pm 4.6$
17	11.0164	0.771	< 1.311	10.4 ± 6.1	$42.0 \pm 24.6 \pm 7.9$	< 1.077	7.7 ± 4.4	$31.1 \pm 17.8 \pm 5.8$
18	11.0175	0.859	< 1.314	8.2 ± 5.2	$29.7 \pm 18.8 \pm 5.7$	< 1.080	1.4 ± 3.4	$5.1 \pm 12.3 \pm 3.4$
19	11.0220	0.982	< 1.323	0.8 ± 4.2	$2.5 \pm 13.3 \pm 3.7$	< 1.091	0.4 ± 3.9	$1.3 \pm 12.4 \pm 4.3$
20	10.8686	22.938	< 0.945	457.5 ± 29.0	$62.1 \pm 3.9 \pm 11.5$	< 0.573	378 ± 42	$51.3 \pm 5.7 \pm 9.5$
21	10.8633	47.647	< 0.930	817.7 ± 32.3	$53.3 \pm 2.1 \pm 9.9$	< 0.545	732 ± 50	$47.8 \pm 3.3 \pm 8.9$
22	10.8667	50.475	< 0.940	999.0 ± 33.0	$61.6 \pm 2.0 \pm 11.5$	< 0.563	820 ± 53	$50.6 \pm 3.3 \pm 9.4$

kinematic limit. The fit returns a B_s yield consistent with zero at each energy point; the measured visible cross section for this sideband region is shown in Fig. 6(c).

The systematic uncertainty for the measured visible cross sections quoted in Table II is dominated by the common multiplicative part due to the uncertainties in the total $e^+e^- \rightarrow b\bar{b}$ cross section and the hadronization fraction f_s . The systematic uncertainty due to the B_s signal yield extraction is determined for each energy point and varies from 6% to 20%.

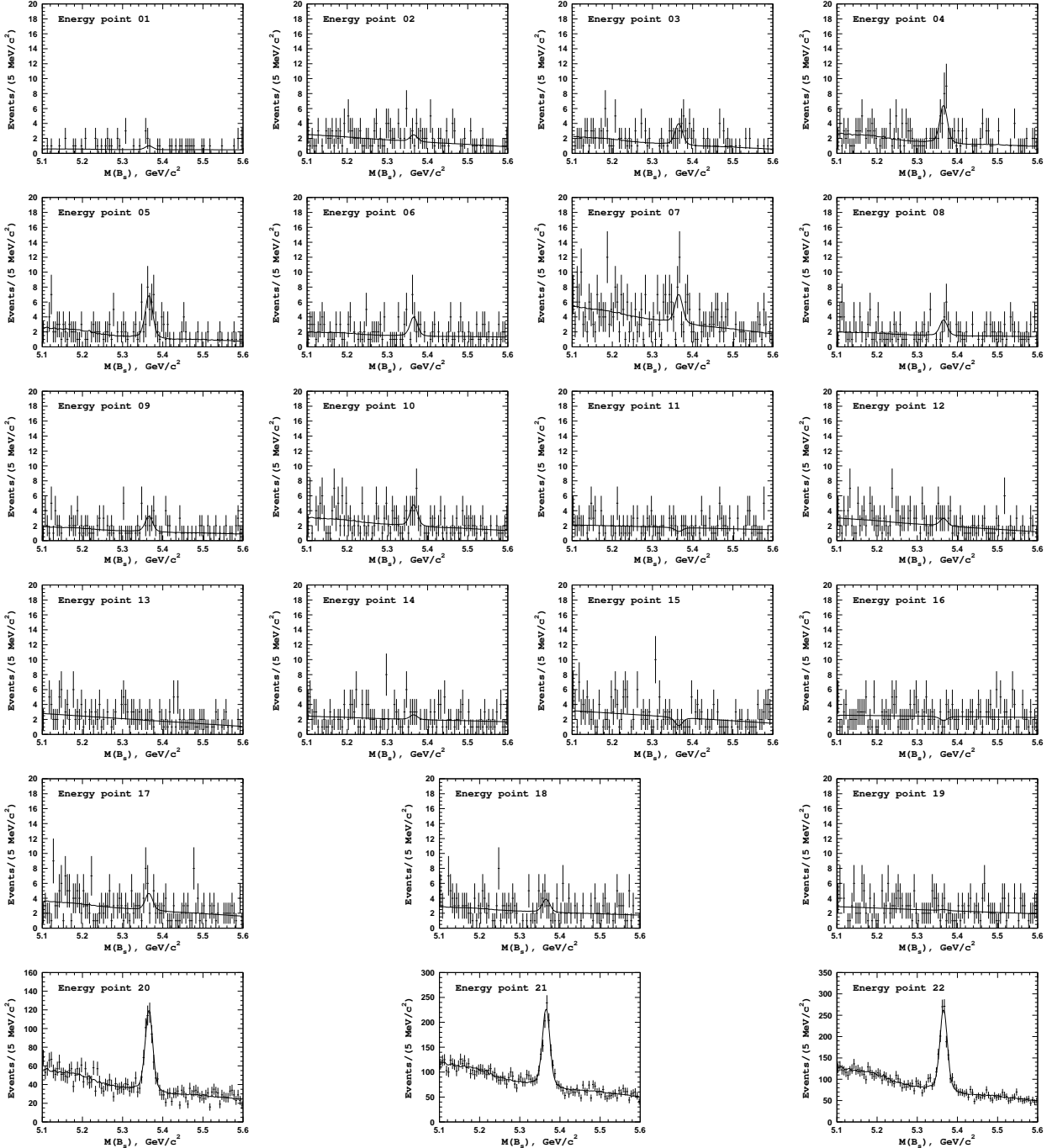


FIG. 5: $M(B_s)$ distributions for $e^+e^- \rightarrow B_s^{(*)}\bar{B}_s^{(*)}$ candidates for each energy point.

CONCLUSION

In conclusion, the ratio of production cross sections for the two-body $B_s^*\bar{B}_s^* : B_s\bar{B}_s^* + c.c.$: $B_s\bar{B}_s$ in e^+e^- annihilation at $\sqrt{s} = 10.866$ GeV is measured to be $7 : 0.853 \pm 0.106 \pm 0.053 : 0.638 \pm 0.094 \pm 0.033$. The fraction of the $S = 0$ component determined from the analysis of

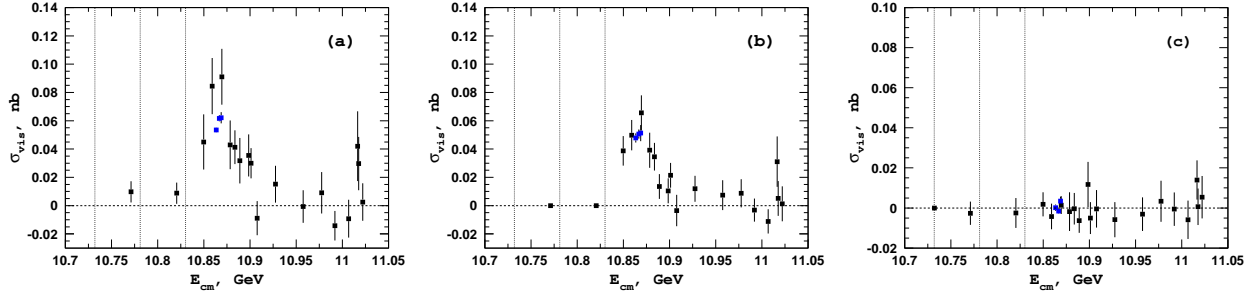


FIG. 6: Cross section for the (a) total $e^+e^- \rightarrow B_s^{(*)}\bar{B}_s^{(*)}$; (b) $e^+e^- \rightarrow B_s^*\bar{B}_s^*$ only; (c) momentum sideband region. Vertical lines show the $B_s\bar{B}_s$, $B_s\bar{B}_s^*$, and $B_s^*\bar{B}_s^*$ thresholds, respectively.

the polar angular distribution of B_s^* produced in the $\Upsilon(10860) \rightarrow B_s^*\bar{B}_s^*$ process is $r = 0.175 \pm 0.057^{+0.022}_{-0.018}$. The measured values of the ratio of the production cross sections and fraction of the $S = 0$ component are in strong contradiction with the HQSS prediction. Some possible reasons for such a difference are discussed in Ref. [12]. Analysis of the $\Upsilon(10860) \rightarrow B_s^*\bar{B}_s^*$ cross section in the energy range from 10.77 to 11.02 GeV reveals a strong signal of the $\Upsilon(10860)$ resonance with no statistically significant signal of the $\Upsilon(11020)$ resonance.

ACKNOWLEDGEMENT

We thank the KEKB group for excellent operation of the accelerator; the KEK cryogenics group for efficient solenoid operations; and the KEK computer group, the NII, and PNNL/EMSL for valuable computing and SINET4 network support. We acknowledge support from MEXT, JSPS, and Nagoyas TLPRC (Japan); ARC and DIISR (Australia); FWF (Austria); NSFC (China); MSMT (Czechia); CZF, DFG, and VS (Germany); DST (India); INFN (Italy); MOE, MSIP, NRF, GSDC of KISTI, and BK21Plus (Korea); MNiSW and NCN (Poland); MES (particularly under Contract No. 14.A12.31.0006) and RFAAE (Russia); ARRS (Slovenia); IKERBASQUE and UPV/EHU (Spain); SNSF (Switzerland); NSC and MOE (Taiwan); and DOE and NSF (U.S.).

- [1] D.Santel *et al.* (Belle Collaboration), Phys. Rev. D **93**, 011101(R) (2016).
- [2] R.Mizuk *et al.* (Belle Collaboration), arXiv:1508.06562 [hep-ex], submitted to PRL.
- [3] A. Abashian *et al.* (Belle Collaboration), Nucl. Instrum. Methods Phys. Res. Sect. A **479**, 117 (2002); also see detector section in J. Brodzicka *et al.* Prog. Theor. Exp. Phys. (2012) 04D001.
- [4] S. Kurokawa and E. Kikutani, Nucl. Instrum. Methods Phys. Res. Sect. A **499**, 1 (2003), and

other papers included in this Volume; T. Abe *et al.* Prog. Theor. Exp. Phys. (2013) 03A001 and following articles up to 03A011.

- [5] D. J. Lange, Nucl. Instrum. Methods Phys. Res. A **462**, 152 (2001).
- [6] E. Barberio and Z. Wąs, Comput. Phys. Commun. **79**, 291 (1994).
- [7] R. Brun *et al.*, GEANT 3.21, CERN Report DD/EE/84-1, 1984.
- [8] K.A. Olive *et al.* (Particle Data Group), Chin. Phys. C **38**, 090001 (2014).
- [9] S. Brandt *et al.*, Phys. Lett. **12**, 57 (1964).
- [10] A. De Rujula, H. Georgi and S. L. Glashow, Phys. Rev. Lett. **38**, 317 (1977).
- [11] M. Voloshin, Phys. Rev. D **85**, 034024 (2012).
- [12] M. Voloshin, Phys. Rev. D **87**, 094033 (2013).
- [13] S. Esen *et al.* (Belle collaboration), Phys. Rev. D **87**, 031101(R) (2013).